Available online at www.sciencedirect.com

SCIENCE DIRECT

Surface & Coatings Technology 200 (2005) 1702 – 1708

SURFACE & COATINGS TECHNOLOGY

www.elsevier.com/locate/surfcoat

# Structural and mechanical properties of nanolayered TiAlN/CrN coatings synthesized by a cathodic arc deposition process

Yin-Yu Chang *, Da-Yung Wang, Chi-Yung Hung

*Department of Materials and Systems Engineering, Mingdao University, Changhua, Taiwan, ROC*

Available online 9 September 2005

**Abstract**

Multilayered TiAlN/CrN as well as monolayered CrN and TiAlN coatings were synthesized by cathodic arc evaporation with plasma enhanced duct equipment, using Cr and $Ti_{50}Al_{50}$ alloy cathodes. Optical emission spectra including atomic and ionized Ti, atomic Al and Cr, excited and ionized nitrogen ($N_2$, $N_2^+$, and $N_2^{2+}$) revealed that excitation, ionization and charge transfer reactions of the Ti–Al–N and Cr–N plasma occurred during the multilayered TiAlN/CrN coating process. The preferred orientation was changed from (200) in CrN and TiAlN monolayered coatings to (111) plane in the multilayered TiAlN/CrN coatings. The multilayered TiAlN/CrN films had smaller crystallite size than the monolayered CrN and TiAlN films. The multilayered TiAlN/CrN coating with periodic thickness of 18 nm exhibited the highest $H^3/E^{*2}$ ratio value of 0.193 GPa, indicating the best resistance to plastic deformation, among the studied CrN, TiAlN and multilayered TiAlN/CrN coatings. The multilayered TiAlN/CrN coatings also showed the best adhesion strength during scratch tests. It has been found that the structural and mechanical properties of the films were correlated with the multiple cathode design and nanolayer thickness.


*Keywords:* TiAlN/CrN; Cathodic arc evaporation; Mechanical properties

## 1. Introduction

Industrial applications of the single layer and multilayer TiAlN coatings synthesized by physical vapor deposition (PVD) are increasing rapidly due to its advanced tribological properties, high temperature oxidation resistance [1,2]. Such coatings can be produced by different PVD techniques, such as magnetron sputtering and cathodic arc evaporation [3,4]. The cathodic arc ion plating process for the deposition of hard coatings is well known for high ionization in the plasma and allows the deposition of dense coatings. The incorporation of aluminum in the cubic fcc TiN structure leads to enhanced thermal stability of the coating [5]. Previous studies revealed that the oxidation resistance of the TiAlN coating for dry cutting applications can be improved by the incorporation of chromium to form Cr-based nitrides which are known for their excellent corrosion and tooling performance [6,7]. This improved high temperature oxidation resistance results in the outperformance of the TiAlCrN-coated cutting tools over the TiAlN-coated cutting tools [2,8]. The periodic thickness and chromium content may influence the microstructure and mechanical properties of the multilayered and nanocomposite TiAlCrN coatings [8,9].

In the present study, a cathodic arc ion plating process with chromium and $Ti_{50}Al_{50}$ alloy cathodes was used for the deposition of CrN, TiAlN, and multilayered TiAlN/CrN coatings. The multilayered TiAlN/CrN coatings in nanoscale periodic thickness were synthesized by rotation of the substrate and use of multi-target geometry. The effects of periodic layer thickness on the microstructure and mechanical properties (hardness, elastic modulus, and adhesion strength) of multilayered TiAlN/CrN coatings were studied.

## 2. Experimental details

CrN, TiAlN, and multilayered TiAlN/CrN coatings were deposited on polished silicon and SKH-51 tool steels (HRc 62) by using a cathodic arc evaporation system. A schematic

* Corresponding author.
*E-mail address:* yinyu@mail2000.com.tw (Y.-Y. Chang).

0257-8972/$ - see front matter © 2005 Elsevier B.V. All rights reserved.
doi:10.1016/j.surfcoat.2005.08.088

figure of the deposition system is illustrated in Fig. 1. Ar and reactive gas ($N_2$) were introduced through a conducting duct around the target to enhance the reaction of the plasma. Emission spectra of the plasma in front of the TiAl and Cr cathodes were recorded in the range from 300 nm to 500 nm using an in-situ optical emission spectrometer (OES, SD2048DL Spectrograph) equipped with a SpectraView application software Version 2.44. A fiber-optic cable, positioned at a distance of 80 mm from the cathode surface, was used for light collection. The optical system employed a 2048 element CCD arrays to obtain a spectral resolution less than 1 nm. The samples were mounted on the rotational substrate holder for the deposition of the CrN, TiAlN, and multilayered TiAlN/CrN coatings. Chromium and Ti/Al (50/50 at.%) alloy targets were arranged on opposite sides of the chamber to deposit the multilayered TiAlN/CrN coatings. The experimental parameters of the deposition process are shown in Table 1. The temperature of the sample during the deposition was measured by a thermocouple located near the sample. The CrN, TiAlN, and multilayered TiAlN/CrN films were deposited at a $N_2$ pressure of 2.5 Pa and substrate bias voltage of −80 V. For the deposition of multilayered TiAlN/CrN films, CrN was deposited as an interlayer. The periodic thickness of the multilayered TiAlN/CrN coating was controlled by the rotational speed of the substrate holder at 2 rpm and 5 rpm.

The deposited multilayered TiAlN/CrN coatings were examined in a Joel JSM-6700F high resolution field emission scanning electron microscope equipped with secondary electron imaging (SEI) and backscattered electron imaging (BEI) detectors. It was operated at an accelerating voltage of 5 kV, and a working distance of 8 mm. Chemical composition of the deposited films was evaluated by Auger Electron Spectroscopy (AES) analyses. It was performed with 3 kV Ar ions to sputter the oxide layer and reveal the chemical composition of the deposited

Table 1
Operating parameters of CrN, TiAlN, and multilayered TiAlN/CrN coatings

| Parameters | Values |
|---|---|
| Base pressure (Pa) | $1.0 \times 10^{-3}$ |
| Reactive gas pressure (Pa) | 2.5 ($N_2$) |
| Deposition time (min) | 40 |
| Distance of cathode to substrate (mm) | 180 |
| CAE target | Cr, $Ti_{50}Al_{50}$ (100 mm in diameter) |
| Cathode current (A) | 80 |
| Bias voltage at ion cleaning stage (V) | −1000 |
| Bias voltage at coating stage (V) | −80 |
| Substrate temperature (°C) | 200–250 |
| Rotational speed of the substrate (rpm) | Monolayered CrN and TiAlN: 5 rpm<br>Multilayered TiAlN/CrN: 2 and 5 rpm |

coating. Glancing angle X-ray diffractometer (Philips X'pert Pro) with a high resolution $\psi$ goniometer and Cu radiation was employed for phase identification and residual stress analysis. The diffractometer was operated at 40 kV and 30 mA with a glancing angle of 2°. The residual stresses of the deposited coatings were calculated from the $\sin^2\psi$ method [10]. According to Williamson–Hall plot method [11–13], contribution of crystallite size and lattice strain to the diffraction line broadening can be calculated through the following two equations:

$$\beta_{hkl} = (\beta_f \cos\Theta)/\lambda \quad (1)$$

$$\beta_{hkl} = (1/D) + (4e/\lambda)\sin\Theta \quad (2)$$

The integral breadth, $\beta_{hkl}$ (expressed in a reciprocal space unit) is related to the integral breadth of the physical broadening, $\beta_f$, which was measured on a $2\Theta$ scale. $\Theta$ is the Bragg's angle of an X-ray reflection. $\lambda$ is the wavelength of X-ray radiation (0.154 nm). $D$ and $e$ are the crystallite size and lattice strain, respectively. Hardness and Young's

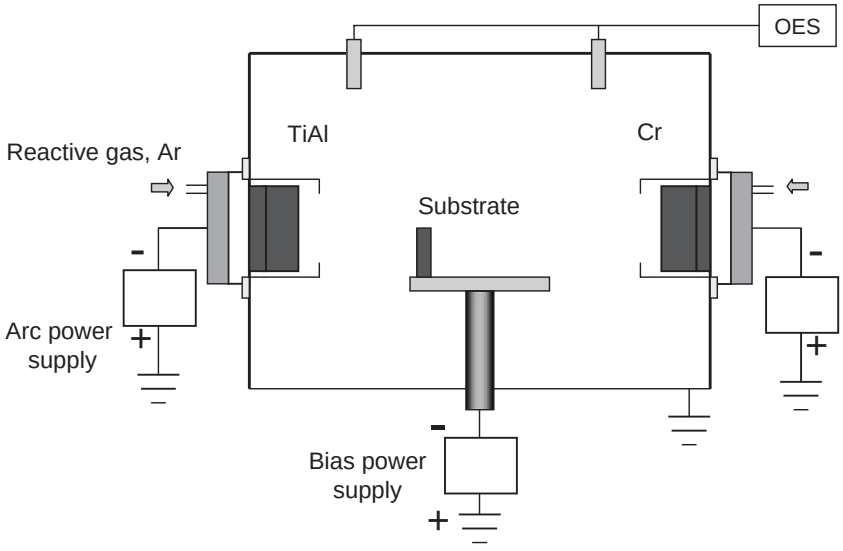


Fig. 1. Schematic diagram of the cathodic arc deposition system.

modulus of the films were obtained using XP-MTS nano-indentation with a Berkovich indenter, under load–unloading condition, and measured as a function of indenter displacement using continuous stiffness measurement method. The maximum penetration depth is controlled at 250 nm. The scratch test and ball-cratering technique were employed to characterize the adhesion strength and failure modes of the deposited coatings. The scratching speed of the indenter was 10 mm/min with a loading rate of 100 N/min from 10 to 80 N. The scratch critical load ($L_c$) of the coating was determined by visual observation using an optical microscope. It was defined as the point at which coating delamination or chipping was first observed, either in or at the edge of the scratch track. The ball crater was ground over the scratch track at scratch load of 55 N of the multilayered TiAlN/CrN coatings to reveal the failure mode of the coating [14,15].

## 3. Results and discussion

### 3.1. Emission spectra of the cathodic arc plasma during the TiAlN/CrN deposition process

Representative Ti–Al–$N_2$ and Cr–$N_2$ emission spectra obtained from the TiAlN/CrN deposition process at arc current of 80 A and bias voltage of −100 V are shown in Fig. 2. The main features of the optical spectra emitted from the plasma, including atomic and ionized Ti, atomic Al and Cr, excited and ionized nitrogen ($N_2$, $N_2^+$, and $N_2^{2+}$) are monitored. In the experiment, titanium appeared in the form of $Ti^+$ ions and excited Ti atoms, while aluminum and chromium appeared as excited Al and Cr atoms. The gaseous component of the generated plasma appeared as both excited and ionized nitrogen when nitrogen gas was introduced. The emission lines of excited and ionized titanium (Ti and $Ti^+$) as well as nitrogen bands ($N_2$, $N_2^+$, and $N_2^{2+}$) indicate the existence of excitation, ionization and charge transfer collisions between titanium ions and neutral nitrogen molecules. Excitation and ionization of the plasma occur to a large extent as a result of collisions between electrons and heavy particles due to the high intensities of the nitrogen bands ($N_2$, $N_2^+$, and $N_2^{2+}$) [16,17]. Periodic TiAlN and CrN were deposited on the substrate depending on the substrate rotation during the multilayered TiAlN/CrN coating process.

### 3.2. Microstructure analysis

From the AES analyses, the composition of the CrN coating deposited from the Cr cathode materials was 58.0 at.% of Cr, 41.5 at.% of N, and 0.5 at.% of oxygen. The composition of the TiAlN coating deposited from the $Ti_{50}Al_{50}$ alloy was 32.3 at.% of Ti, 23.8 at.% of Al, 43.1 at.% of N, and 0.8 at.% of oxygen. An atomic ratio of Al/(Ti+Al) in the TiAlN film was reduced to 0.42 compared

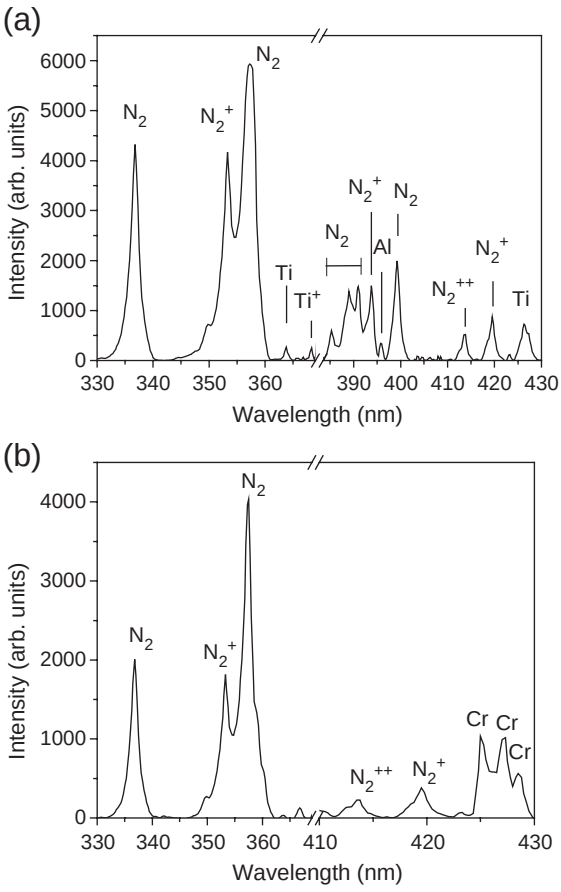


Fig. 2. Optical emission spectra of the cathodic arc plasma obtained in front of the (a) TiAl and (b) Cr cathodes ranging from 330 to 430 nm during the deposition of the multilayered TiAlN/CrN coating.

with the $Ti_{50}Al_{50}$ cathode material. It can be related to the lower atomic mass of Al that suffers higher scattering in the collisions with nitrogen, and leads to a lower volume density in the vapor [18,19]. Typical X-ray diffraction spectra from the CrN, TiAlN, and multilayered TiAlN/CrN coatings deposited at 2 rpm (TiAlN/CrN-2 rpm) and 5 rpm (TiAlN/CrN-5 rpm) of rotational speeds are shown in Fig. 3. The result revealed that the monolayered CrN and TiAlN displayed a preferred (200) orientation parallel to the substrate surface. The multilayered TiAlN/CrN coatings also exhibited the B1-NaCl crystal structure. However, the preferred orientation was changed from (200) in CrN and TiAlN to (111) plane in the TiAlN/CrN coatings. The peak positions represented the weighted mean of the individual reflections from the TiAlN and CrN phases. The (200) diffraction peak was asymmetric because of the presence of TiAlN and CrN components. Higher fraction of CrN phase in (200) plane was found in the TiAlN/CrN coating deposited at lower rotational speed of 2 rpm. This indicated that the CrN component of the film would influence the development of the {200} texture in the multilayered TiAlN/CrN coatings deposited at different rotational speed of substrate. It also revealed a competitive growth between CrN and TiAlN in multi-

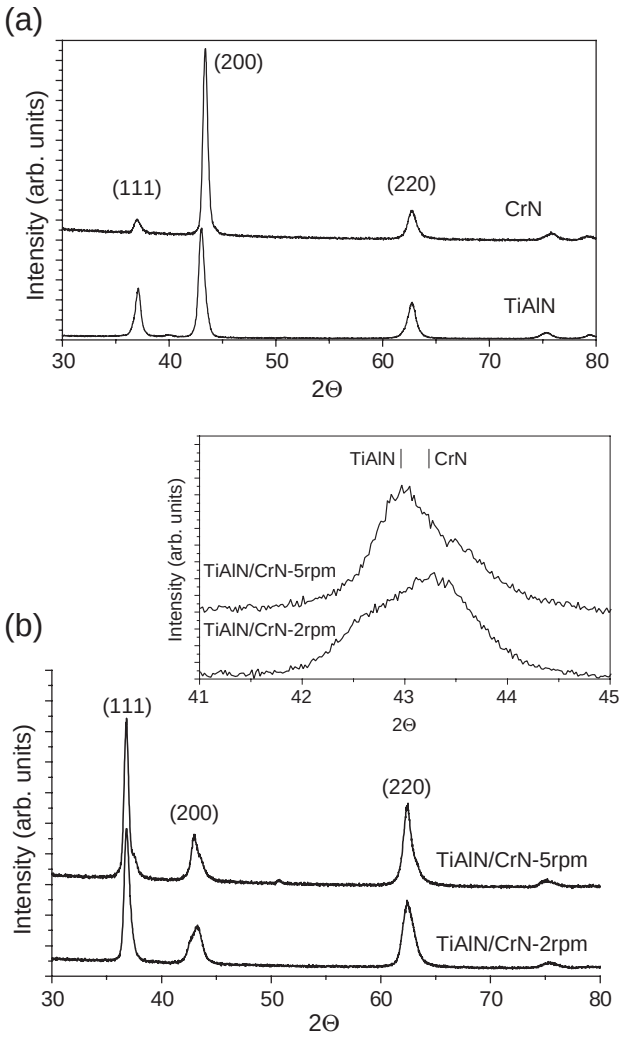


Fig. 3. X-ray diffraction spectra of the CrN and TiAlN coatings (a), and multilayered TiAlN/CrN coatings deposited at 2 and 5 rpm (b).

layered TiAlN/CrN coatings at different rotational speed of substrate.

Cross-sectional secondary and backscattered SEM micrographs showing the structure of the TiAlN/CrN multilayered coatings deposited at 2 rpm and 5 rpm rotational speeds are shown in Fig. 4. The film thickness was 1.8 μm, and the deposition rate was about 0.045 μm/min. The coating had a dense columnar structure typical of the zone T according to the zone classification proposed by Thornton [20]. This structure resulted from the ion-induced defects, such as point defect clusters and small dislocation loops being trapped in the film and hence leading to a continuous re-nucleation of new grains during growth that disrupted the columnar microstructure. Cross-sectional SEM micrograph of the multilayer obtained with backscattered electron detector emphasized the dissimilarity between CrN and TiAlN. CrN produced more backscattered electrons, and was displayed as layers with brighter contrast. The multilayer coating revealed a stacking of CrN and TiAlN layers. This coating consisted of a CrN interfacial layer and a periodic structure of superlattice TiAlN/CrN layers. The backscattered electron image revealed the periodic thickness of 18 nm and 7 nm in the multilayered TiAlN/CrN coatings deposited at 2 and 5 rpm, respectively. The distinct multilayered structure can be found in the TiAlN/CrN deposited at rotational speed of 2 rpm, as shown in Fig. 4(a). However, the layered microstructure of TiAlN/CrN deposited at 5 rpm, as shown in Fig. 4(b), was not as clear as that shown in Fig. 4(a). The interface between the TiAlN and CrN was not sharp because of the interlayer diffusion.

The crystallite size and lattice strain of the deposited films calculated from the Williamson–Hall plot are shown in Table 2. The crystallite size of monolayered CrN and TiAlN is 48 nm and 41 nm, respectively. The multilayered TiAlN/CrN films had smaller crystallite size than the monolayered CrN and TiAlN films. The multilayered TiAlN/CrN coating deposited at 2 rpm possessed the smallest crystallite size of 31 nm among the deposited coatings. The smaller crystallite size was controlled by the interface phenomena [21]. Substrate rotation during the film production was used to control the time that the substrate is under ion bombardment from different cathodes (Cr and TiAl). Thus, the film growth is interrupted by each layer. In this manner, nanolayers can be obtained with different mechanical properties, which may enhance the film hardness. However, the crystallite size in the multilayered coating deposited at 5 rpm should be smaller than that in the coating deposited at 2 rpm. The larger crystallite size in the multilayered coating deposited at 5 rpm is probably due to the broad interfaces induced by interlayer diffusion during the cathodic arc deposition process. The value of lattice strain was larger in multilayered TiAlN/CrN coatings than in CrN and TiAlN coatings. It indicates a larger structural anisotropy at the atomic level in TiAlN/CrN multilayered layers, probably connected with the nano-scale multilayered columnar texture.

### 3.3. Mechanical properties

Hardness and elastic modulus of the CrN, TiAlN, and multilayered TiAlN/CrN coatings deposited on SKH-51 tool steels were measured as a function of indenter displacement using continuous stiffness measurement method, as shown in Table 2. The hardness values shown in Table 2 correspond to the indentation depth of approximately 0.2–0.3 μm, where the influence of the substrate is negligible. The hardness of the CrN and TiAlN is 24 and 31 GPa, respectively. The multilayered TiAlN/CrN coatings exhibited a higher hardness of 36–37 GPa. The presence of the nanolayered structure of the TiAlN/CrN coatings can increase the hardness based on the dislocation blocking by layer interfaces and Hall–Petch effect [9,21–25]. In order to increase the resistance to plastic deformation, it is desirable to obtain materials that possess high hardness but lower elastic modulus values. This behavior is then well expressed by the $H^3/E^{*2}$ ratio, where $H$ and $E^*$ are the hardness and

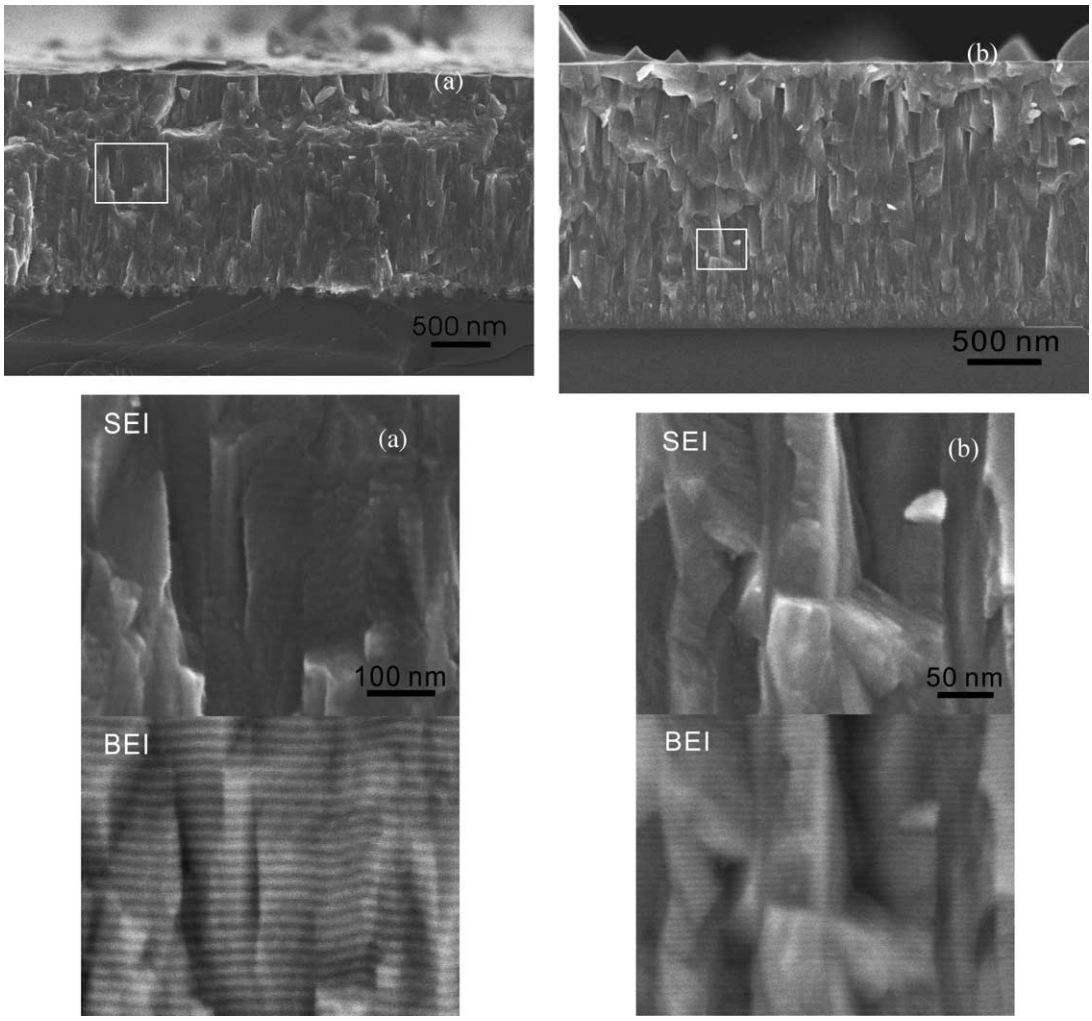


Fig. 4. Cross-sectional secondary and backscattered SEM micrographs showing the structure of the TiAlN/CrN multilayered coatings deposited at 2 rpm (a) and 5 rpm (b).

effective modulus of the coating. $E^*$ could be further expressed as $E^*=E/(1-\nu^2)$, where $E$ is the Young's modulus, and $\nu$ is the Poisson ratio ($\sim 0.25$) [26–28]. With higher $H$ and lower $E^*$, the plastic deformation is lower, because the external load is distributed over a larger area and the stress distribution is more uniform. The multilayered TiAlN/CrN coatings exhibited higher $H^3/E^{*2}$ ratio than that of CrN (0.114) and TiAlN (0.081) coatings. The $H^3/E^{*2}$ ratio showed the highest value of 0.193 GPa for the TiAlN/CrN multilayered coating deposited at 2 rpm among the studied coatings. The $H^3/E^{*2}$ ratio was enhanced by the interface contribution of the multilayered TiAlN/CrN. This provides higher resistance to plastic deformation of the multilayered TiAlN/CrN with periodic thickness of 18 nm.

Table 2
Crystallite size, lattice strain, hardness, elastic modulus, $H^3/E^{*2}$, residual stress, and critical load of the CrN, TiAlN, and multilayered TiAlN/CrN coatings deposited on SKH-51 tool steels

| Coatings | CrN | TiAlN | TiAlN/CrN-5 rpm | TiAlN/CrN-2 rpm |
|---|---|---|---|---|
| Crystallite size (nm) | 48 | 41 | 38 | 31 |
| Lattice strain (nm) | $4.3\times10^{-3}$ | $4.3\times10^{-3}$ | $4.9\times10^{-3}$ | $5.7\times10^{-3}$ |
| Elastic modulus (GPa) | 290 | 570 | 520 | 480 |
| Hardness (GPa) | 24 | 31 | 36 | 37 |
| $H^3/E^{*2}$ (GPa) | 0.144 | 0.081 | 0.152 | 0.193 |
| Residual stress (GPa) | −6.6 | −5.4 | −11.2 | −10.1 |
| Critical load (N) | 45 | 35 | 46 | 50 |

The residual stresses of the CrN, TiAlN, and multilayered TiAlN/CrN coatings, which were determined by the $\sin^2\psi$ method and the measured elastic modulus, are also revealed in Table 2. The difference in magnitude was related to the residual stress which composed of an intrinsic component resulted from the growth process and an extrinsic component (thermal stress) due to the presence of different thermal expansion coefficients between the coating and the substrate. The higher compressive residual stress was found in the multilayered TiAlN/CrN coating with higher hardness. The multilayered TiAlN/CrN coating deposited at 2 rpm with periodic thickness of 18 nm possessed lower residual stress of −10.1 GPa than TiAlN/CrN coating (−11.2 GPa) deposited at 5 rpm with periodic

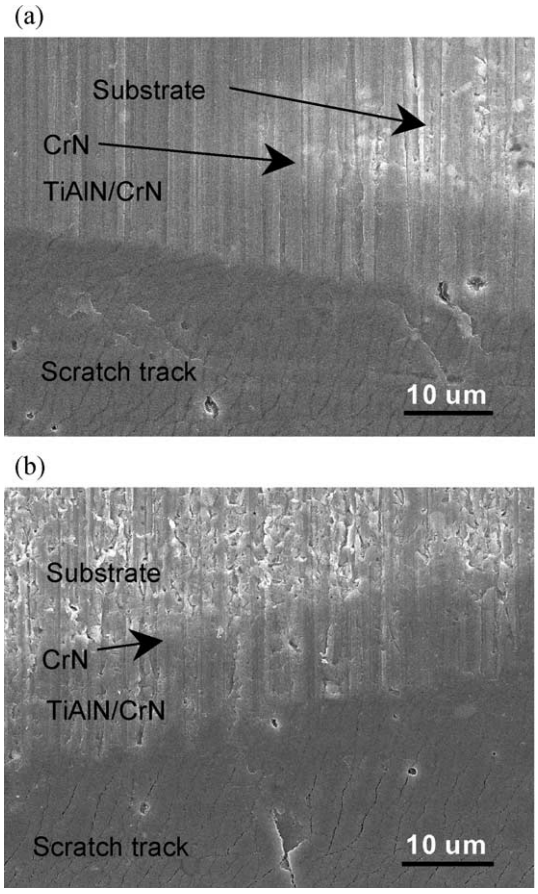


Fig. 5. Ball crater on the scratch track at 55 N of the TiAlN/CrN coatings deposited at 2 rpm (a) and 5 rpm (b). The taper section revealed by the ball crater shows that the diamond indenter produced plastic deformation of the substrate. The coating deformed with the substrate and without being penetrated.

thickness of 7 nm. The stress behavior shows a relaxation effect of the multilayered TiAlN/CrN coating with larger periodic thickness of 18 nm.

The scratch test revealed the lowest critical load of 35 N for the TiAlN coating, as shown in Table 2. Higher critical load was revealed in the CrN and multilayered TiAlN/CrN coatings. Higher adhesion strength can be obtained by the deposition of CrN and multilayered TiAlN/CrN coatings synthesized by the cathodic arc deposition process which was used in this study. The multilayered TiAlN/CrN coating deposited at 2 rpm possessed the highest critical load of 50 N. The failure mode of the TiAlN/CrN coatings deposited on SKH-51 tool steels was revealed by a ball crater ground over the scratch track at the scratch load position of 55 N, as shown in Fig. 5. The taper section revealed by the ball crater shows that the diamond indenter produced plastic deformation of the substrate. The coating deformed with the substrate and without being penetrated. Although some surface cracks were visible at 55 N load, no crack paths were found within the TiAlN/CrN layer, at the interface between TiAlN/CrN layer and CrN layer, and at the interface with substrate. The ability of the multilayered TiAlN/CrN coating to deform with the substrate and the condition of the interfaces without cracking reveals excellent adhesion and toughness of the coating.

## 4. Conclusions

1. In this study, multilayered TiAlN/CrN and monolayered CrN, TiAlN coatings were synthesized by cathodic arc evaporation. Optical emission spectra including atomic and ionized Ti, atomic Al and Cr, excited and ionized nitrogen ($N_2$, $N_2^+$, and $N_2^{2+}$) revealed that excitation, ionization and charge transfer reactions of the Ti–Al–$N_2$ and Cr–$N_2$ plasma occurred during the multilayered TiAlN/CrN coating process. Periodic thickness of the multilayered coatings was controlled by the substrate rotation speed. All of the CrN, TiAlN and multilayered TiAlN/CrN coatings exhibited the B1-NaCl crystal structure. Monolayered CrN and TiAlN coatings showed a preferred (200) orientation parallel to the substrate surface. In the multilayered TiAlN/CrN coatings, however, (111) preferential orientation was exhibited. The competitive growth of CrN and TiAlN in multilayered TiAlN/CrN coatings resulted in the smallest crystallite size in the TiAlN/CrN coating with periodic thickness of 18 nm among the studied CrN, TiAlN, and multilayered TiAlN/CrN coatings.
2. The multilayered TiAlN/CrN coatings possessed higher hardness of 36–37 GPa than that of the monolayered CrN (24 GPa) and TiAlN (31 GPa) coatings. The nanolayered structure of the TiAlN/CrN coatings is responsible for the hardness enhancement due to the smaller crystallite size based on the Hall–Petch effect. The highest $H^3/E^{*2}$ ratio of 0.193 GPa, indicating the best resistance to plastic deformation, was achieved in the TiAlN/CrN coating deposited at 2 rpm among the studied coatings. The best adhesion strength was also obtained in this multilayered TiAlN/CrN coating.

## Acknowledgements

The authors wish to thank Mr. Shein-Chen Liu from Surftech Corp. for generously providing the CAE deposition system to accomplish all the experiments. In addition, the authors would like to thank Mr. Yu-Fong Lu of the National Chung-Hsing University for providing FESEM analysis. The funding in part from the National Science Council of Taiwan under the contract NSC-93-2622-E-451-001-CC3 is sincerely appreciated.

## References

[1] S. Paldey, S.C. Deevi, Mater. Sci. Eng., A 342 (2003) 58.
[2] S.G. Harris, E.D. Doyle, A.C. Vlasveld, J. Audy, D. Quick, Wear 254 (2003) 723.

[3] W.D. Münz, L.A. Donohue, P.Eh. Hovsepian, Surf. Coat. Technol. 125 (2000) 269.
[4] F. Weber, F. Fontaine, M. Scheib, W. Bock, Surf. Coat. Technol. 177–178 (2004) 227.
[5] H.G. Prengel, A.T. Santhanam, R.M. Penich, P.C. Jindal, K.H. Wendt, Surf. Coat. Technol. 94–95 (1997) 597.
[6] I. Wadsworth, I.J. Smith, L.A. Donohue, W.D. Münz, Surf. Coat. Technol. 94–95 (1997) 315.
[7] M.I. Lembke, D.B. Lewis, W.D. Münz, Surf. Coat. Technol. 125 (2000) 263.
[8] K. Yamamoto, T. Sato, K. Takahara, K. Hanaguri, Surf. Coat. Technol. 174–175 (2003) 620.
[9] A.E. Santana, A. Karimi, V.H. Derflinger, A. Schutze, Surf. Coat. Technol. 177–178 (2004) 334.
[10] C.H. Ma, J.H. Huang, Haydn Chen, Thin Solid Films 418 (2002) 73.
[11] G.K. Williamson, W.H. Hall, Acta Metall. 1 (1953) 22.
[12] V. Valvoda, R. Kužel Jr., R. Černý, Thin Solid Films 156 (1988) 53.
[13] B.S. Yau, J.L. Huang, D.F. Lii, P. Sajgalik, Surf. Coat. Technol. 177–178 (2004) 209.
[14] S. Yang, A.H.S. Jones, D.G. Teers, Surf. Coat. Technol. 133–134 (2000) 369.
[15] P. Panjan, M. Cekada, B. Navinsek, Surf. Coat. Technol. 174–175 (2003) 55.
[16] R.L. Boxman, D.M. Sanders, P.J. Martin, J.M. Lafferty, Handbook of Vacuum Arc Science and Technology, Noyes, New Jersey, 1995.
[17] J. Bujak, J. Walkowicz, J. Kusinski, Surf. Coat. Technol. 180–181 (2004) 150.
[18] R. Wuhrer, W.Y. Yeung, Scr. Mater. 49 (2003) 199.
[19] J.M. Lackner, W. Waldhauser, R. Ebner, R.J. Bakker, Appl. Phys., A 79 (2004) 1469.
[20] J.A. Thornton, Annu. Rev. Mater. Sci. 7 (1977) 239.
[21] P.C. Yashar, W.D. Sproul, Vacuum 55 (1999) 179.
[22] S.J. Bull, A.M. Jones, Surf. Coat. Technol. 78 (1996) 173.
[23] Xi Chu, Scott A. Barnett, J. Appl. Phys. 77 (1995) 4403.
[24] M. Shinn, S.A. Barnett, Appl. Phys. Lett. 64 (1994) 61.
[25] H. Holleck, V. Schier, Surf. Coat. Technol. 76–77 (1995) 328.
[26] T.Y. Tsui, G.M. Pharr, W.C. Oliver, C.S. Bhatia, R.L. White, S. Anders, A. Anders, I.G. Brown, Mater. Res. Soc. Symp. Proc. 383 (1995) 447.
[27] J. Musil, F. Kunc, H. Zeman, H. Polakova, Surf. Coat. Technol. 154 (2002) 304.
[28] A. Leyland, A. Matthews, Wear 246 (2000) 1.